CrossMark

TOPICAL COLLECTION: INTERNATIONAL CONFERENCE ON THERMOELECTRICS 2018

Preparation of Tetrahedrite $Cu_{12}Sb_4S_{13}$ by Mechanical Alloying and Hot Pressing

SUNG-YOON KIM,[1] SUNG-GYU KWAK,[1] JI-HEE PI,[1] GO-EUN LEE,[1] and IL-HO KIM[1,2]

1.—Department of Materials Science and Engineering, Korea National University of Transportation, Chungju 27469, Korea. 2.—e-mail: ihkim@ut.ac.kr

Tetrahedrite $Cu_{12}Sb_4S_{13}$ was synthesized via mechanical alloying (MA) and consolidated using hot pressing (HP) as a solid-state route. Powders with a single phase of $Cu_{12}Sb_4S_{13}$ could be successfully synthesized without post-annealing by controlling the process conditions of MA: 350 rpm for 24 h in an Ar atmosphere. A sintered tetrahedrite with density close to the theoretical density was obtained via HP at 723 K for 2 h under a pressure of 70 MPa. Thermogravimetric and calorimetric analyses confirmed weight loss and endothermic reactions at temperatures above 853 K, possibly due to the decomposition/melting of the tetrahedrite and the volatilization/melting of the constituent elements. The synthesized tetrahedrite is a nondegenerate semiconductor; its electrical conductivity increased with the increase in temperature. Its Seebeck coefficient also increased with the increase in temperature without showing intrinsic conduction up to 773 K. As the HP temperature increased, the power factor decreased because the decrease in the electrical conductivity prevailed over the increase in the Seebeck coefficient. The thermal conductivity had similar low values regardless of the HP temperature. The maximum dimensionless figure-of-merit, $ZT_{max} = 0.87$, was obtained at 723 K for the $Cu_{12}Sb_4S_{13}$ hot-pressed at 723 K.

Key words: Thermoelectric, tetrahedrite, mechanical alloying, hot pressing

INTRODUCTION

Tetrahedrites are attractive, cost-effective, and earth-abundant p-type thermoelectric materials which exhibit high dimensionless figure-of-merit (ZT) values near 723 K.[1,2] One of the most striking features of tetrahedrites is their extremely low thermal conductivity of 0.55 $Wm^{-1} K^{-1}$ at temperatures above 300 K. The tetrahedrite $Cu_{12}Sb_4S_{13}$ has a complex crystal structure with 58 atoms arranged in a highly symmetric cubic unit cell (space group: $I\bar{4}3m$) composed of CuS_4 tetrahedra, CuS_3 triangles, and SbS_3 trigonal pyramids.[3] Cu^{II} atoms experience fluctuating bonding interactions with the lone-pair electrons of Sb atoms and thus anharmonically vibrate out of the CuS_3 plane at low

frequency and high amplitude, leading to low lattice thermal conductivity.[4–6] From a crystallographic point of view, the cubic tetrahedral phase $Cu_{10}^{1+}Cu_2^{2+}Sb_4^{3+}S_{13}^{2-}$ has a cubic structure in which the Cu^I and Cu^{II} atoms are different from each other. In general, one-third of Cu^I is occupied by monovalent copper cations and two-thirds by divalent copper cations, whereas the Cu^{II} position is filled with monovalent cations.[7] The low lattice thermal conductivity is mainly related to the Cu^{II} site, whereas the substitution of divalent cations at the Cu^I site primarily affects the electrical resistivity, thereby reducing the charge carrier contribution to thermal conductivity.[8–10]

Generally, when tetrahedrite is synthesized using a melting process, a sophisticated and slow reaction (heating–maintaining–cooling) is required because the boiling point of S is lower than the melting point of Cu. In addition, a long-time heat treatment is

required for phase transformation and homogenization. Mechanical alloying (MA) has several advantages—such as the prevention of phase separation during melting—over conventional melt-crushing techniques, and it has been applied to the synthesis of nano-sized powders.[11] Lu and Morelli[12] reported a single-phase tetrahedrite solid solution prepared by high-energy ball milling of the pure elements, Cu, Sb and S, with the natural mineral tetrahedrite, where the natural mineral served as a seed matrix and incorporated pure elements into a parent compound. Barbier et al.[13] combined a high-energy ball-milling procedure and elemental precursors with spark plasma sintering, and could considerably reduce the total processing time. In this study, the optimum process conditions for MA and hot pressing (HP) were investigated to prepare the basic ternary tetrahedrite $Cu_{12}Sb_4S_{13}$, and its phase transformation and thermoelectric properties were examined.

EXPERIMENTAL

$Cu_{12}Sb_4S_{13}$ powder was synthesized via MA. Elemental powders of Cu (purity 99.9%, $< 45 \mu$m; Kojundo), Sb (purity 99.999%, $< 150 \mu$m; Kojundo), and S (purity 99.99%, $< 75 \mu$m; Kojundo) were mixed and loaded into a hardened stainless-steel jar with stainless-steel balls of diameter 5 mm. The ball-to-powder weight ratio was 20. MA was performed at 300–400 rpm for 12–48 h in an Ar atmosphere using a planetary mill (Fritsch Pulverisette5). The synthesized tetrahedrite powder was charged into a graphite mold with an inner diameter of 10 mm and subjected to HP at 673–773 K for 2 h under 70 MPa in vacuum.

The phases of the MA powders and HP specimens were analyzed using x-ray diffraction (XRD; Bruker D8-Advance) with Cu Kα radiation (λ = 0.15405 nm). The diffraction patterns were measured in the θ–2θ
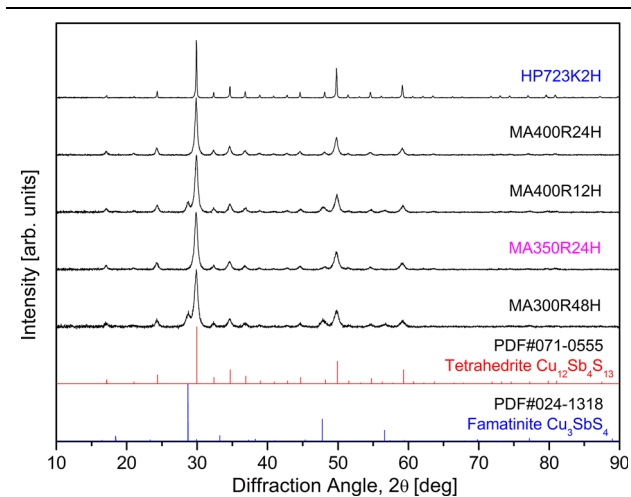

Fig. 1. XRD patterns of synthetic powders and sintered specimens prepared using mechanical alloying and hot pressing.

Table I. Chemical compositions, physical properties, and charge transport parameters of $Cu_{12}Sb_4S_{13}$ at room temperature

Specimen	Composition		Relative density (%)	Lattice constant (nm)	FWHM$_{(222)}$ (deg)	Hall coefficient (cm³ C⁻¹)	Mobility (cm² V⁻¹ s⁻¹)	Carrier concentration (10^{20} cm⁻³)	Lorenz number (10^{-8} V² K⁻²)
	Nominal	Actual							
MA350R24H	$Cu_{12}Sb_4S_{13}$	$Cu_{12.34}Sb_{4.18}S_{12.48}$	–	1.0327	0.505	–	–	–	–
HP723K2H	$Cu_{12}Sb_4S_{13}$	$Cu_{12.48}Sb_{4.13}S_{12.39}$	99.2	1.0327	0.127	0.02	4.35	3.12	1.71–1.81

mode ($2\theta = 10°–90°$) with a step size of 0.02° and scan speed of 0.4 s/step. A scanning electron microscope (SEM; FEI Quanta400) and energy-dispersive x-ray spectrometer (EDS; Bruker Quantax200) were used to observe the raw materials used in MA and the $Cu_{12}Sb_4S_{13}$ powders synthesized using MA, and to analyze the polished and fractured surfaces of the HP specimens. The weight changes and phase transitions of the MA powders and HP specimens were analyzed using thermogravimetry and differential scanning calorimetry (TG-DSC; Mettler Toledo TG/DSC1), in which the temperature was increased to 950 K at a heating rate of 5 K/min in an Ar atmosphere.

The Hall coefficient, carrier concentration, and mobility of the HP specimens were measured using the van der Pauw method (Keithley 7065) under a magnetic field of 1 T and electric current of 50 mA at room temperature. The thermoelectric properties were examined in the temperature (T) range 323-723 K. The Seebeck coefficient (α) and electrical conductivity (σ) were measured using the temperature differential method and the DC four-probe method (Ulvac-Riko ZEM-3). The thermal conductivity (κ) was obtained from the thermal diffusivity, specific heat, and density, which were measured using the laser flash method (Ulvac-Riko TC-9000H). The power factor (PF) and dimensionless figure of merit (ZT) were evaluated using the relationships $PF = \alpha^2\sigma$ and $ZT = \alpha^2\sigma\kappa^{-1}T$, respectively.

RESULTS AND DISCUSSION

Figure 1 shows the XRD patterns of the synthetic tetrahedrites according to the MA–HP conditions. MA at 300 rpm for up to 48 h (MA300R48H) did not yield a single phase of tetrahedrite ($Cu_{12}Sb_4S_{13}$), and a secondary phase of famatinite (Cu_3SbS_4) coexisted. However, a single tetrahedrite phase was successfully synthesized at 350 rpm for 24 h (MA350R24H). In order to shorten the time required for MA, its speed was increased to 400 rpm for 12 h (MA400R12H), but the famatinite phase was still present. Thus, the optimal MA conditions in this study were determined to be 350 rpm for 24 h. The tetrahedrite phase synthesized using MA (MA350R24H) remained after HP—i.e., the XRD peaks of only the tetrahedrite phase were identified for the sintered specimen hot-pressed at 723 K for 2 h (HP723K2H). The XRD peaks of the MA powders were broad owing to the fine particle size and stress induced during the MA process. However, the diffraction peaks of the HP specimens became sharper which could be
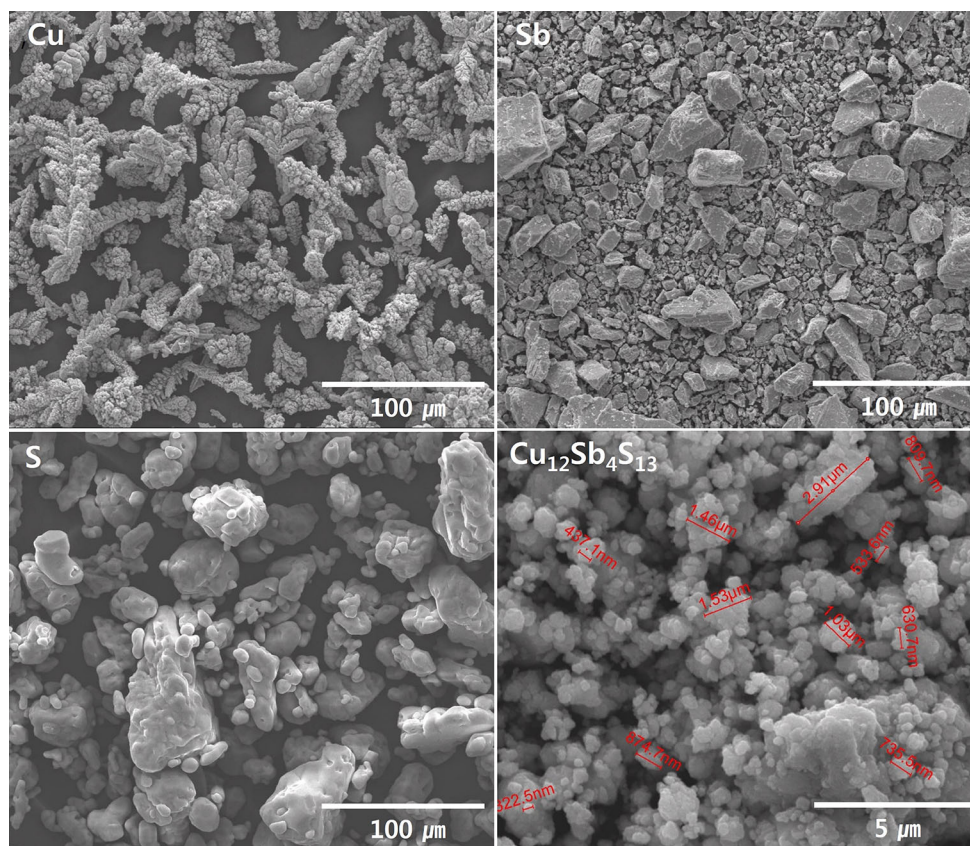

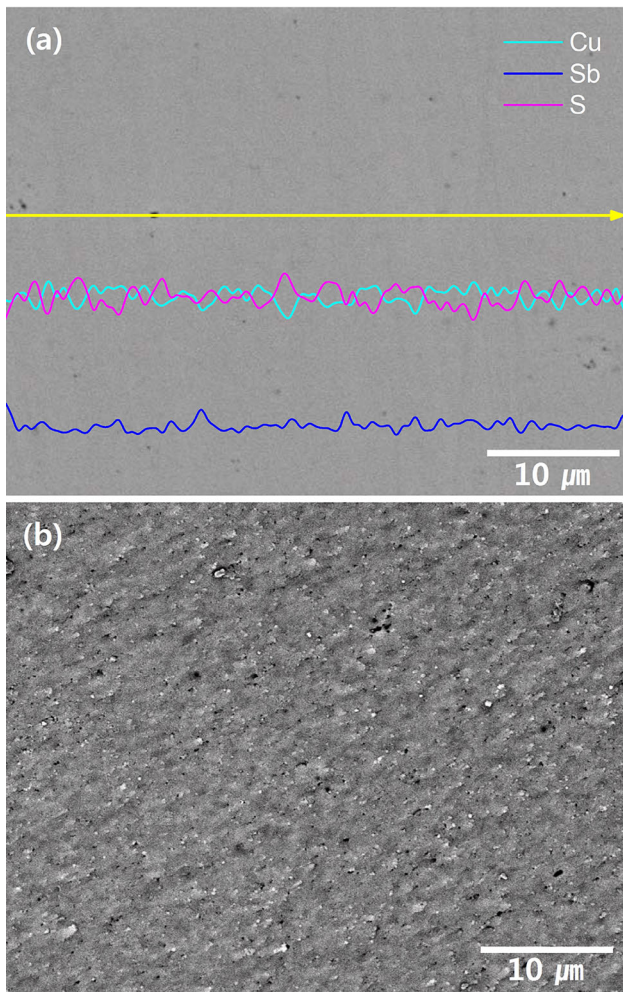Fig. 2. SEM images of raw materials (Cu, Sb, and S) and synthetic tetrahedrite powder.

Fig. 3. SEM images and EDS line scans of (a) the polished surface and (b) the fractured surface of the specimen hot-pressed at 723 K for 2 h.

Fig. 4. Analyses of (a) TG and (b) DSC of the $Cu_{12}Sb_4S_{13}$ powder mechanically alloyed at 350 rpm for 24 h and the sintered specimen hot-pressed at 723 K for 2 h.

interpreted to be as a result of grain growth and stress release during the HP process. As presented in Table I, the full width at half maximum (FWHM) of the diffraction peak for the (222) plane was significantly reduced, from 0.505° for MA350R24H to 0.127° for HP723K2H.

Figure 2 shows the SEM images of the raw material powders (Cu, Sb, and S) and the tetrahedrite powder synthesized using MA. The particle sizes of the raw powders were less than 150 μm as supplied by the manufacturers, and the average particle size of the synthetic powder obtained after MA was reduced to several μm. Figure 3 shows the microstructures observed in the back-scattered electron mode and EDS line scans of the polished and fractured surfaces of the HP specimen (HP723K2H). A sound specimen was obtained with a high relative density of 99.2% compared with the theoretical density (4.99 g cm^{-3})[14] of tetrahedrite. In addition, no secondary phase was observed, and the constituent elements were homogeneously distributed.

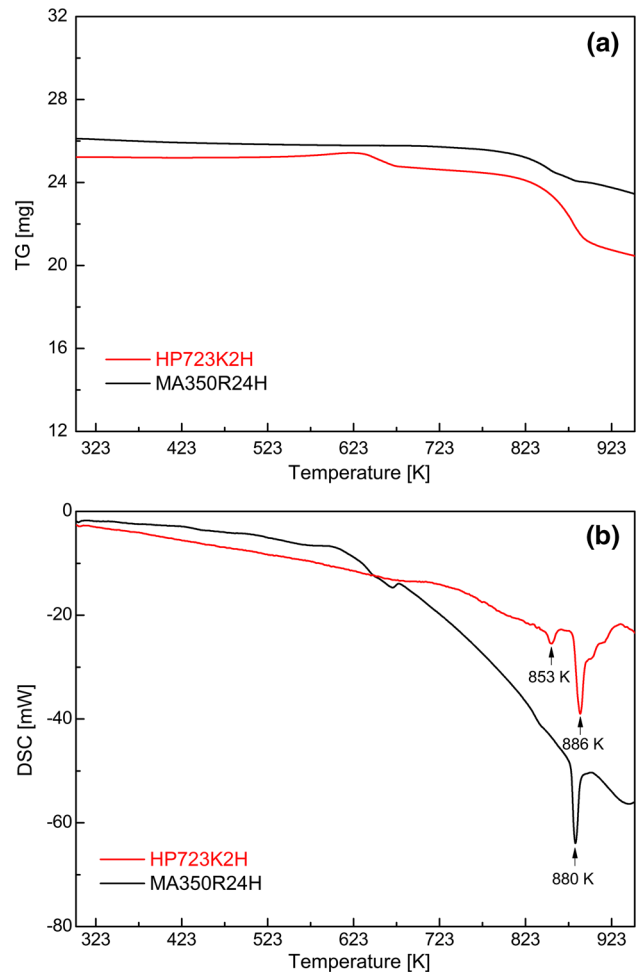Figure 4 shows the results of TG-DSC analyses of the MA powder and HP specimen. Weight loss occurred at temperatures above 823 K, possibly owing to the decomposition of tetrahedrite (phase transformation) and the volatilization of constituent elements via melting. Endothermic reactions were observed at 880 K for the MA powder and at 886 K for the HP specimen, and these temperatures corresponded to the melting point of tetrahedrite. The HP specimen underwent an endothermic reaction at 853 K, which is considered the decomposition temperature of the tetrahedrite.[15] The thermal stability of the tetrahedrite determined using the TG-DSC analysis has rarely been reported.[16–18] The undoped $Cu_{12}Sb_4S_{13}$ was reported to melt incongruently, decomposing at temperatures above 816 K into digenite (Cu_2S), famatinite (Cu_3SbS_4), and skinnerite (Cu_3SbS_3).[19]

Table I lists the chemical composition, physical properties, and charge transport parameters of $Cu_{12}Sb_4S_{13}$ prepared using the MA–HP process. The actual compositions of the synthetic powder and sintered specimen were similar to the nominal
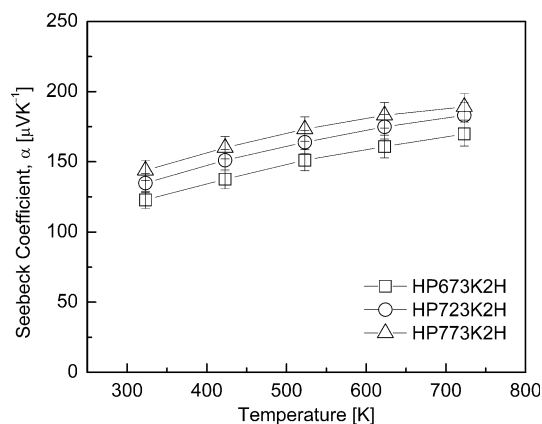
Fig. 5. Temperature dependence of the Seebeck coefficient of the hot-pressed tetrahedrites.

Fig. 7. Temperature dependence of the power factor of the hot-pressed tetrahedrites.
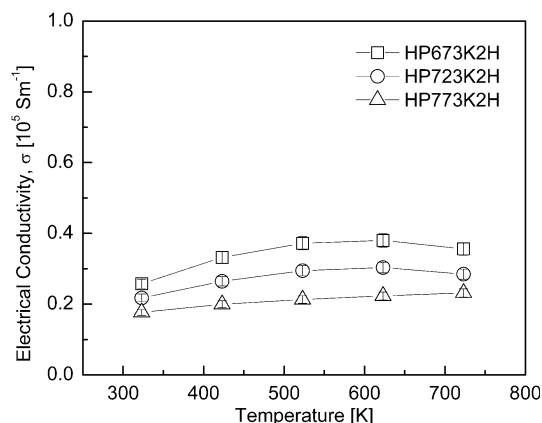

Fig. 6. Temperature dependence of the electrical conductivity of the hot-pressed tetrahedrites.

composition, but the composition of S was found to be slightly deficient. The lattice constant was calculated to be 1.0327 nm. The Hall coefficient of undoped Cu$_{12}$Sb$_4$S$_{13}$ showed a positive sign, which indicated a p-type semiconductor with holes acting as charge carriers. The carrier concentration of the HP723K2H specimen was 3.12×10^{20} cm^{-3} at room temperature.

The temperature dependences of the thermoelectric properties were examined for the specimens HP673K2H, HP723K2H, and HP773K2H sintered at various HP temperatures from 673 K to 773 K. Figure 5 shows the Seebeck coefficient (α) of the mechanically alloyed and hot-pressed Cu$_{12}$Sb$_4$S$_{13}$. The Seebeck coefficient of a p-type semiconductor is expressed as $\alpha = (8/3)\pi^2 k_B^2 m^* T e^{-1} h^{-2} (\pi/3n)^{2/3}$, where k_{B} is the Boltzmann constant, m^* the effective carrier mass, e the electronic charge, h Planck's constant, and n the carrier concentration.[20] As the temperature rises, the Seebeck coefficient increases; however, a significant increase in the carrier concentration owing to the intrinsic transition at a certain temperature leads to a decrease in the
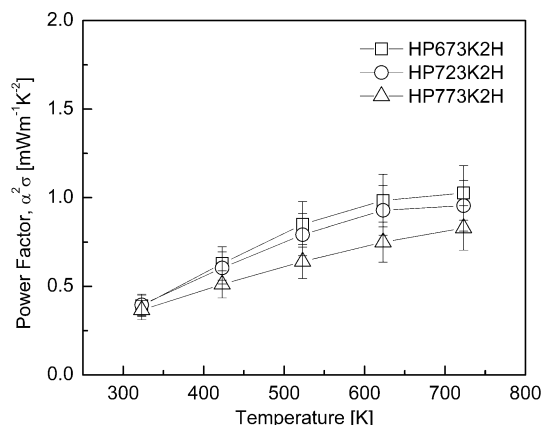
Seebeck coefficient; therefore, the Seebeck coefficient has a peak value at a specific temperature. As shown in Fig. 5, the Seebeck coefficient increased with the increase in temperature up to 723 K, and, thus, the intrinsic transition temperature of Cu$_{12}$Sb$_4$S$_{13}$ was estimated to be higher than the measuring temperature range employed in this study. As the HP temperature increases, the Seebeck coefficient also slightly increases. The HP773K2H specimen showed high values of the Seebeck coefficient, ranging from 143.3 μV K^{-1} to 189.2 μ VK^{-1} in the temperature range 323–723 K.

Figure 6 shows the electrical conductivity (σ) of Cu$_{12}$Sb$_4$S$_{13}$. A positive temperature dependence of the electrical conductivity in the measuring temperature range indicates nondegenerate semiconductor behavior. The electrical conductivity of Cu$_{12}$Sb$_4$S$_{13}$ decreased with the increase in HP temperature. The higher the processing (e.g., annealing or sintering) temperature, the more is the change in the carrier concentration owing to the volatilization of elements, especially S.[21] For the HP673K2H specimen, the highest electrical conductivity of 2.6×10^4–3.8×10^4 S m^{-1} was obtained at temperatures ranging from 323 K to 723 K.

Figure 7 shows the power factor (PF) of Cu$_{12}$Sb$_4$S$_{13}$. The PF value increases in proportion to the Seebeck coefficient and electrical conductivity as PF $= \alpha^2 \sigma$.[22] However, both the Seebeck coefficient and electrical conductivity depend on the carrier concentration; these two parameters have a trade-off relationship. Therefore, optimizing the carrier concentration is necessary to obtain the maximum PF value, which can be achieved by doping suitable atoms at the Cu, Sb, and/or S sites. In this study, the PF value increased with the increase in temperature owing to the increases in both the Seebeck coefficient and electrical conductivity. The intrinsic transition did not occur in the measuring temperature range, and, thus, the PF value increased with the increase in temperature. The
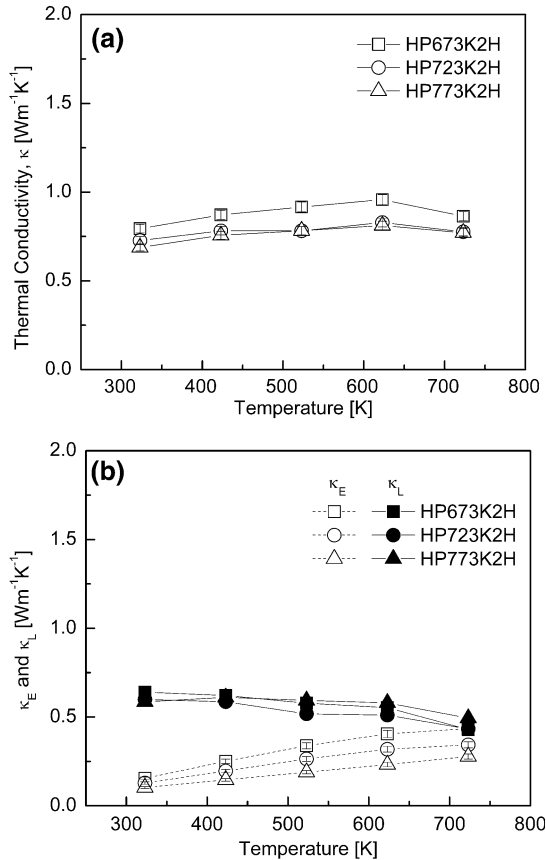
Fig. 8. Temperature dependence of the thermal conductivities of the hot-pressed tetrahedrites: (a) total thermal conductivity and (b) electronic and lattice thermal conductivities.

Fig. 9. Dimensionless figure-of-merit of the synthetic tetrahedrites.

PF values decreased with the increase in HP temperature. This was because the reduction in the electric conductivity dominated the increase in the Seebeck coefficient. HP673K2H showed a PF of 0.4 mW m^{-1} K^{-2} at 323 K, but the maximum PF was 1.0 mW m^{-1} K^{-2} at 723 K.

Figure 8 shows the thermal conductivity (κ) of Cu$_{12}$Sb$_4$S$_{13}$. The thermal conductivity is the sum of the electronic thermal conductivity (κ_E) and lattice thermal conductivity (κ_L). The electronic thermal conductivity was calculated using the Wiedemann–Franz law ($\kappa_E = L\ \sigma T$, L: Lorenz number),[23] and thus, the lattice thermal conductivity could be separated. The Lorenz number was estimated using the equation $L = 1.5 + \exp^{-|\alpha|/116}$, where the units of L and α are 10^{-8} V^2 K^{-2} and μV K^{-1}, respectively.[24] For instance, L was calculated to be 1.71×10^{-8} V^2 K^{-2} to 1.81×10^{-8} V^2 K^{-2} at temperatures ranging from 323 K to 723 K, as presented in Table I. The HP773K2H specimen showed the lowest thermal conductivity of 0.69–0.81 W m^{-1}K^{-1} in the measuring temperature range, because the carrier concentration was low and κ_E was the lowest. The κ_L values of all the specimens were very low, with similar values regardless of the HP temperature: κ_L = 0.59–0.60 W m K^{-1} at 323 K,

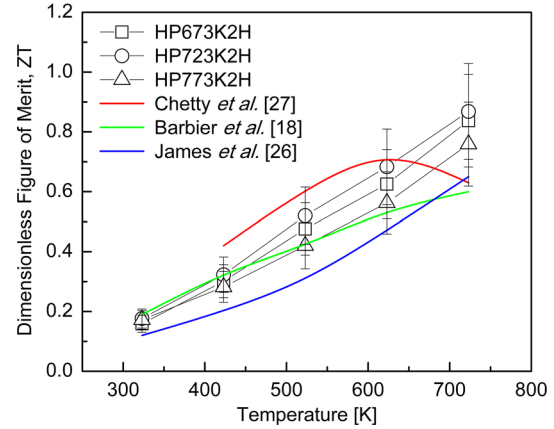and κ_L = 0.43–0.49 W m K^{-1} at 723 K. This low thermal conductivity of the tetrahedrite Cu$_{12}$Sb$_4$S$_{13}$ results from the complex crystal structure in which Cu is located at two different sites; Cu$^{\mathrm{I}}$ is coordinated to the tetrahedral by the S atom and Cu$^{\mathrm{II}}$ is coordinated to the triangular by the S atom. The low thermal conductivity was reported to be due to the effect of the lone-pair electrons of Sb, and similar phenomena occur in similar compounds such as CuSbSe$_2$ and Cu$_3$SbSe$_3$.[25]

Figure 9 shows the dimensionless ZT of Cu$_{12}$Sb$_4$S$_{13}$. The ZT value increased with the increase in temperature because the PF value increased and the thermal conductivity remained low without intrinsic transition. HP723K2H exhibited the maximum ZT, $ZT_{\max} = 0.87$ at 723 K, although the power factor and thermal conductivity varied slightly depending on the HP temperature. The ZT values of undoped tetrahedrites were compared to the literature. Barbier et al.[18] achieved $ZT_{\max} = 0.60$ at 723 K for Cu$_{12}$Sb$_4$S$_{13}$ synthesized via encapsulated melting and spark plasma sintering. James et al.[26] reported $ZT_{\max} = 0.65$ at 723 K for Cu$_{12}$Sb$_4$S$_{13}$ prepared via solvothermal synthesis and hot pressing. Chetty et al.[27] achieved $ZT_{\max} = 0.75$ at 623 K for Cu$_{12}$Sb$_4$S$_{13}$ fabricated via encapsulated melting and hot pressing, but this value decreased at temperatures above 623 K, resulting in $ZT = 0.63$ at 723 K. In our study, Cu$_{12}$Sb$_4$S$_{13}$ prepared via MA and HP as a solid-state route exhibited excellent thermoelectric performance of $ZT = 0.56$–0.68 at 623 K and $ZT = 0.76$–0.87 at 723 K.

CONCLUSIONS

The ternary tetrahedrite Cu$_{12}$Sb$_4$S$_{13}$ was successfully and easily synthesized via MA. A single tetrahedrite phase could be obtained via MA at 350 rpm for 24 h. Homogeneous and dense consolidation could be performed using HP at 673–773 K for 2 h under 70 MPa. No phase transition was observed after HP and no post-annealing was

required. All the specimens showed positive Hall and Seebeck coefficients and exhibited p-type characteristics. The tetrahedrite could be applied at temperatures above 723 K because phase decomposition and intrinsic transition did not occur at 723 K. The thermoelectric performance varied slightly with the change in HP temperature. In the case of the specimen hot-pressed at 723 K, a superior dimensionless ZT = 0.87 at 723 K was obtained. MA and HP were confirmed to be useful and practical methods for the solid-state synthesis and sintering of tetrahedrite via a relatively fast process.

ACKNOWLEDGEMENT

REFERENCES

1. X. Lu and D.T. Morelli, *Phys. Chem. Chem. Phys.* 15, 5762 (2013).
2. X. Lu, D.T. Morelli, Y. Xia, F. Zhou, V. Ozolins, H. Chi, X. Zhou, and C. Uher, *Adv. Energy Mater.* 3, 342 (2013).
3. A. Pfitzner, M. Evain, and V. Petricek, *Acta Crystallogr.* 53, 337 (1997).
4. Y. Bouyrie, C. Candolfi, S. Pailhès, M.M. Koza, B. Malaman, A. Dauscher, J. Tobola, O. Boisron, L. Saviot, and B. Lenoir, *Phys. Chem. Chem. Phys.* 17, 19751 (2015).
5. W. Lai, Y. Wang, D.T. Morelli, and X. Lu, *Adv. Funct. Mater.* 25, 3648 (2015).
6. E. Lara-Curzio, A.F. May, O. Delaire, M.A. McGuire, X. Lu, C.Y. Liu, E.D. Case, and D.T. Morelli, *J. Appl. Phys.* 115, 193515 (2014).
7. F. Di Benedetto, G.P. Bernardini, C. Cipriani, C. Emiliani, D. Gatteschi, and M. Romanelli, *Phys. Chem. Miner.* 32, 155 (2005).
8. N.E. Johnson, J.R. Craig, and J.D. Rimstidt, *Am. Miner.* 73, 389 (1988).
9. K. Friese, A. Grzechnik, E. Makovicky, T. Balic-Zunic, and S. Karup-Møller, *Phys. Chem. Miner.* 35, 455 (2008).
10. K. Suekuni, K. Tsuruta, M. Kunii, H. Nishiate, E. Nishibori, S. Maki, M. Ohta, A. Yamamoto, and M. Koyano, *J. Appl. Phys.* 113, 043712 (2013).
11. Y.Q. Yu, B.P. Zhang, Z.H. Ge, P.P. Shang, and Y.X. Chen, *Mater. Chem. Phys.* 131, 1 (2011).
12. X. Lu and D.T. Morelli, *MRS Commun.* 3, 129 (2013).
13. T. Barbier, S. Rollin-Martinet, P. Lemoine, F. Gascoin, A. Kaltzoglou, P. Vaqueiro, A.V. Powell, and E. Guilmeau, *J. Am. Ceram. Soc.* 99, 51 (2016).
14. J.W. Anthony, R.A. Bideaux, K.W. Bladh, and M.C. Nichols, *Handbook of Mineralogy*, Vol. I (Chantilly: Mineralogical Society of America, 2003).
15. M.H. Braga, J.A. Freerira, C. Lopes, and L.F. Malheiros, *Mater. Sci. Forum* 587, 435 (2008).
16. Y. Bouyire, C. Candolfi, V. Ohorodniichuk, B. Malaman, A. Dauscher, J. Tobola, and B. Lenoir, *J. Mater. Chem. C* 3, 10476 (2015).
17. A.P. Gonçalves, E.B. Lopes, J. Monnier, J. Bourgon, J.B. Vaney, A. Piarristeguy, A. Pradel, B. Lenoir, G. Delaizir, M.F.C. Pereira, E. Alleno, and C. Godart, *J. Alloys Compd.* 664, 209 (2016).
18. T. Barbier, P. Lemine, S. Gascoin, O. Lebedev, A. Kaltzoglou, P. Vaqueiro, A.V. Powell, R.I. Smith, and E. Guilmeau, *J. Alloys Compd.* 634, 253 (2015).
19. F.D. Luce, E. Makovicky, and B.J. Skinner, *Econ. Geol.* 67, 924 (1972).
20. G.J. Snyder and E.S. Toberer, *Nat. Mater.* 7, 105 (2008).
21. X.A. Fan, J.Y. Yang, R.G. Chen, H.S. Yun, W. Zhu, S.Q. Bao, and X.K. Duan, *J. Phys. D* 39, 740 (2006).
22. X. Yan, B. Poudel, Y. Ma, W. Liu, G. Joshi, H. Wang, Y. Lan, D. Wang, G. Chen, and Z. Ren, *Nano Lett.* 10, 3373 (2010).
23. H. Cailat, A. Borshchevsky, and J.P. Fleurial, *J. Appl. Phys.* 80, 4442 (1996).
24. B. Madaval and S.J. Hong, *Electron. Mater.* 45, 12 (2016).
25. R. Chetty, A. Bali, and R.C. Mallik, *J. Mater. Chem. C* 3, 12364 (2015).
26. D.J. James, X. Lu, D.T. Morelli, S.L. Brock, and A.C.S. Appl, *Mater.* 7, 23623 (2015).
27. R. Chetty, P. Kumar, G. Rogl, P. Rogl, E. Bauer, H. Michor, S. Suwas, S. Pucjegger, G. Giester, and R.C. Mallik, *Phys. Chem. Chem. Phys.* 17, 1716 (2015).